Optical Materials: X 24 (2024) 100372

Contents lists available at ScienceDirect

Optical Materials: X

journal homepage: www.journals.elsevier.com/optical-materials-x

Scintillation properties of multilayered composite scintillators based on the YAG:Ce and TbAG:Ce single crystalline films and GAGG:Ce crystal substrates

Y. Syrotych [a,b,*], V. Gorbenko [a], S. Witkiewicz-Łukaszek [a], T. Zorenko [a], M. Kaczmarek [b], J. Pejchal [c], J.A. Mares [c], R. Kucerkova [c], M. Nikl [c], K. Kamada [d], A. Yoshikawa [d], Yu Zorenko [a]

[a] Department of Physics, Kazimierz Wielki University in Bydgoszcz, 85090, Bydgoszcz, Poland
[b] Department of Mechatronics, Kazimierz Wielki University in Bydgoszcz, 85-074, Bydgoszcz, Poland
[c] Institute of Physics, Academy of Sciences of Czech Republic, 16200, Prague, Czech Republic
[d] Institute for Materials Research, Tohoku University, 2-1-1 Katahira, Aoba-ku, Sendai, 980-8577, Japan

A B S T R A C T

This work demonstrates current progress of our group in developing of two- and three-layered composite for radiation monitoring of various components of mixed ionization radiation fluxes based on the epitaxial structures of Ce^{3+} doped garnet compounds using the Liquid Phase Epitaxy growth technique. These scintillators contain one or two single crystalline films, dedicated for registration of low-penetrating particles, and bulk single crystal substrates used for detection of high-penetrating γ-rays. For creation of two- and three-layered epitaxial structures, the single crystalline films of Ce^{3+} doped $Y_3Al_5O_{12}$, $Tb_3Al_5O_{12}$ and $Tb_2GdAl_5O_{12}$ garnets were used. The single crystal of mixed $Gd_3Ga_xAl_{5-x}O_{12}$:Ce garnet with fixed Ga concentrations of x = 2.3 and 3.0 are utilized as substrates. To assess the scintillation properties of these epitaxial structures, the pulse height spectra, light yield and scintillation decay kinetics were measured under excitation by α–particles (^{239}Pu), β-particles (^{90}Sr + ^{90}Y) and γ–rays (^{137}Cs). Finally, the figure-of merit of composite scintillators under study were calculated for selection of the best epitaxial structures for simultaneous registration α– and β-particles and γ–rays.

1. Introduction

A major step forward in the creation of "phoswich" detectors for radiation monitoring in various applications was made with the development of composite scintillators using the liquid phase epitaxy (LPE) growth method [1–9]. Such composite scintillators grown using the LPE method enable the simultaneous recording and analysis of many components of mixed ionizing radiation, including particles and quanta with different penetration depths. Recently, more and more information has been published about the development of two- and three-layer composite scintillators consisting of films and crystals of different scintillation materials forming completely single-crystalline epitaxial structures synthesized by the LPE method [10,11]. Single crystalline films (SCFs) and single crystals (SCs) of various oxide compounds, such as garnets, perovskites, and ortho- and pyrosilicates, serve as the main basis for these scintillators [12–14].

An essential characteristic of these materials in film and crystal form is their ability to scintillate under various types of ionizing fluxes. For effective detecting high-energy and high-penetrating γ-quanta, such scintillators should possess high density and large effective atomic number (Z_{eff}). Therefore, along all heavy scintillators, we consider the $Gd_3Al_2Ga_3O_{12}$:Ce (GAGG:Ce) garnet with density ρ = 6.63 g/cm^3 and Z_{eff} = 54.4, as one of the promising candidates for bulk crystal part of composite scintillator [15]. Remarkably, the GAGG:Ce crystals exhibit relatively high light yield (LY) of approximately 46,000 photons per MeV and an energy resolution up to 7.8 % at 662 keV γ-rays excitation [16]. Additionally, the crystals of such a garnet can be synthesized with different gallium concentrations, varying from 2.3 up to 3.0 formula units. This means that the GAGG:Ce crystals with different Ga concentration stands out as an excellent choice as a substrate for developing of different types of SCFs and composite scintillators using the LPE technique.

Using the LPE method, it is possible to create epitaxial structures containing SCFs with various lattice constants, dopants, and thicknesses. Specifically, short-range penetrating α-particles from ^{239}Pu and ^{241}Am sources and medium penetrating β-particles of ^{90}Sr+^{90}Y source can be stopped in the epitaxial structures of garnet compounds consisting of one "light" SCF with thickness of 12–15 μm and "heavy" SC substrate with thickness about of 0.8–1.2 mm, or epitaxial structures containing two SCF scintillators grown step-by-step on the same SC substrate. In the

* Corresponding author.
E-mail address: syr@ukw.edu.pl (Y. Syrotych).

https://doi.org/10.1016/j.omx.2024.100372
Received 30 April 2024; Received in revised form 9 September 2024; Accepted 1 October 2024
Available online 9 October 2024
2590-1478/© 2024 The Author(s). Published by Elsevier B.V. This is an open access article under the CC BY-NC-ND license (http://creativecommons.org/licenses/by-nc-nd/4.0/).

last case, the thickness of the second SCF layer, dedicated mainly for registration of β-particles must be *as large as possible*, and material for preparation of this film must be completed from high density/high Z_{eff} compounds. However, technological limitation of LPE method enable growth process of good quality SCF scintillators with thickness typically not overcoming 50–100 μm. Due to such limitation the choice of the type of material for the second SCF layer dedicated for β-particles registration is a large challenge in our research.

The registration of different components of ionizing radiation can be accomplished using the difference of scintillation decay curves originated from different parts of composite scintillator [10,11]. In this case, the different penetration abilities of high-energy particles and quanta in a multilayer structure result is the different scintillation decay kinetics arising in different parts of the SCF&SC composite structure. It provides a unique opportunity for clear separation of various types of ionizing radiation in the active scintillation recording mode. Taking into account the features of the scintillation properties of GAGG:Ce substrates discussed above, it makes sense to develop SCFs from other types of garnets. The $Y_3Al_5O_{12}$:Ce (YAG:Ce) and $Tb_3Al_5O_{12}$:Ce (TbAG:Ce) garnets are a good choice for this application because they have rather different scintillation decay kinetics compared to GAGG:Ce garnet. Namely, the decay time of Ce^{3+} luminescence in YAG host is about of 70 ns, when the main component of Ce^{3+} luminescence decay in TbAG:Ce host is much slower in the hundreds ns range. The "light" YAG:Ce SCF scintillator with density 4.5 g/cm^{-3}, effective atomic number 29 and thickness in the 12–15 μm range is suitable for full stopping of α-particles with energy of 5.15–5.5 MeV [11,12]. In the opposite, the choice of TbAG:Ce garnet as the best second SCF scintillator for the detection of β-particles is strongly supported by other characteristic of this material, such as high density of 5.96 g/cm^{-3} and effective atomic number of 53.25.

Important peculiarity of TbAG:Ce SCF crystallization with lattice constant 12.073 Å is the possibility of LPE growth both onto YAG substrates with smaller lattice constant of 12.006 A, as well as onto GAGG SCF substrates with Ga content x = 2.5 ($GAGG_{2.5}$:Ce) and lattice constant of 12.231 Å. The SCF/substrate misfit $\mathbf{m} = (\mathbf{a}_{SCF} - \mathbf{a}_{sub}/\mathbf{a}_{sub})*100$ % in these cases was equal to 0.7 % and 1.8 %, respectively [17]. Due to that the TbAG:Ce SCF/GAGG:Ce SC composite scintillators was also created using LPE method. Such type of composite scintillator shows very good characteristics for simultaneous registration α-particles and γ-rays in the mixed ionization fluxes [10,11] and can be used as an initial epitaxial structure for the creation of three-layered composite scintillators for simultaneous registration α- and β-particles and γ-rays.

$GAGG_x$:Ce SCF substrates with other Ga concentration of x = 2.3 ($GAGG_{2.3}$:Ce) and x = 3.0 ($GAGG_{3.0}$:Ce) and lattice constant of 12.260 Å and a = 12.259 Å, respectively, can also be used for creation of doubly- and triply-layered composite scintillators. The application of these substrates gives additional possibility for suitable tuning of the scintillation decay kinetics of substrates with respect the decay kinetics of SCF scintillators. Meanwhile, it is expected that the SCF/substrate misfit in this case does not overcome the critical 1.6 % limit, suitable for stable LPE growth performance. Namely, in this work we used $GAGG_{2.3}$:Ce SC substrates for LPE growth of doubly-layered TbAG:Ce $SCF_1/GAGG_{2.3}$:Ce SC and triply-layered YAG:Ce SCF_2/TbAG:Ce $SCF_1/GAGG_{2.3}$ SC composite scintillators. However, in the case of $GAGG_3$:Ce SC substrates with large Ga content, the TbAG:Ce SCF cannot be directly crystalized on them due to large SCF/substrate misfit above 1.6 %. For this reason, with aim of decreasing the misfit value, the Gd alloying in TbAG host was used. Specifically, doubly-layered $Tb_2GdAl_5O_{12}$:Ce (Tb_2GdAG:Ce) $SCF_1/GAGG_3$:Ce SC and triply-layered YAG:Ce SCF_2/Tb_2GdAG:Ce $SCF_1/GAGG_3$:Ce SC with different SCF thickness were crystalized in this work and their optical and scintillation properties were investigated. The obtained results were compared to determine the composition with best figure of merit (FOM) for detection of three type of ionization radiation including α- and β-particles and γ-rays.

2. Samples and experimental technique

Preparation of samples for this study consisted of several stages. The first step was to create $GAGG_{2.3}$:Ce and $GAGG_{3.0}$:Ce SCs substrates. The Czochralski growth method was used to produce such crystals at the IMR Tohoku University in Japan. As previously noted, the gallium concentration in the solid solution, which fluctuates between 2.3 and 3.0 formula units, strongly limits the content of crystals grown using this technique.

The growth of first sample sets (S1) of doubly-layered composite scintillators based on the TbAG:Ce SCF_1 and Tb_2GdAG:Ce SCF_1 onto $GAGG_{2.3}$:Ce and $GAGG_3$:Ce SC substrates were performed using the LPE technique [18,19]. The second set (S2) of three-layered composite scintillators based on the YAG:Ce SCF_2 and TbAG:Ce $SCF_1/GAGG_3$:Ce SC and Tb_2GdAG:Ce $SCF_1/GAGG_3$:Ce SC epitaxial structures as "substrates" was created using same LPE technique. Growth SCFs with different thicknesses, in range from 22 μm up to 52 μm as s first SCF in S1 set, and 22 μm up to 26 μm as a second SCF in S2 set (Fig. 1), allows us to control the penetration depth of α- and β-particles in the film parts of composite scintillator during excitation with various types of radiation. Controlling the SCFs thickness provides flexibility in choosing the best composite composition for effective simultaneous detection of α- and β-particles and γ-rays.

For this study it was essential to characterize the scintillation properties of composite scintillators in comparison to other well-known scintillation materials. For this purpose, a reference sample of YAG:Ce SCF was selected with known LY of 2650 photons/MeV under excitation with α–particles of ^{239}Pu source (Table 1). Table 1 shows that the $GAGG_x$:Ce SC substrates have a high LY that is within 3.1–3.6 times large than that of the reference YAG:Ce SCF. At the same time, the LY of the samples from S1 group remains higher compared to the reference sample but significantly lower in comparison with the $GAGG_x$:Ce SC substrates. Instead, LY of SCF part of S2 set shows much lower LY values than the YAG:Ce SCF reference sample. This effect can be explained by a strong influence of Pb^{2+} flux related dopant due to using melt-solution based on the $PbO–B_2O_3$ flux during LPE growth of SCF scintillators [11,20].

For characterization of the luminescent and scintillation properties of SCFs and bulk SC parts of composite scintillators, absorption spectra, cathodoluminescence (CL) spectra, pulse height spectra (PHS), light yield (LY) and scintillation decay kinetics under α– (^{239}Pu), β- (^{90}Sr) particles and γ– rays (^{137}Cs) sources were measured. The absorption spectra were measured using a Jasco 760 UV–Vis spectrometer within 200–1100 nm wavelength range. CL spectra of SCFs and SCs in the 200–1200 nm range were measured using a JEOL JSM-820 scanning electron microscope with an electron beam energy of 20 kV. Initial measurements of scintillation LY and decay kinetics for SCF parts of composite scintillators were performed using a setup comprising a Hamamatsu H6521 photomultiplier, multichannel analyser, Tektronix TDS3052 digital oscilloscope, and substrate YAG:Ce as reference sample (Table 1). Fitting the scintillation decay traces were performed using a three-exponential model, representing distinct fast, intermediate, and slow decay stages, by adjusting the amplitudes and time constants to best match the experimental data. Scintillation decay time on $t_{1/e}$, $t_{1/10}$ and $t_{1/20}$ levels (Table 1) were calculated using this fitting. Subsequently, Pulse Height Spectra (PHS) measurements for these composite scintillators were carried out at the Institute of Physics, Czech Academy of Science in Prague using a setup with a hybrid PMT (HPMT DEP PP0475B with pre-amplifier), measuring electronics (Ortec 672 Spectroscopy Amplifier and 927 ASPEC MCA), and PC control. The SCF and SC substrate samples were excited using α-particles from a^{239}Pu source with an energy of 5.15 MeV, β-particles from a^{90}Sr source (546 keV), and γ-quanta from a^{137}Cs source (661.7 keV). All measurements were conducted at room temperature (RT).

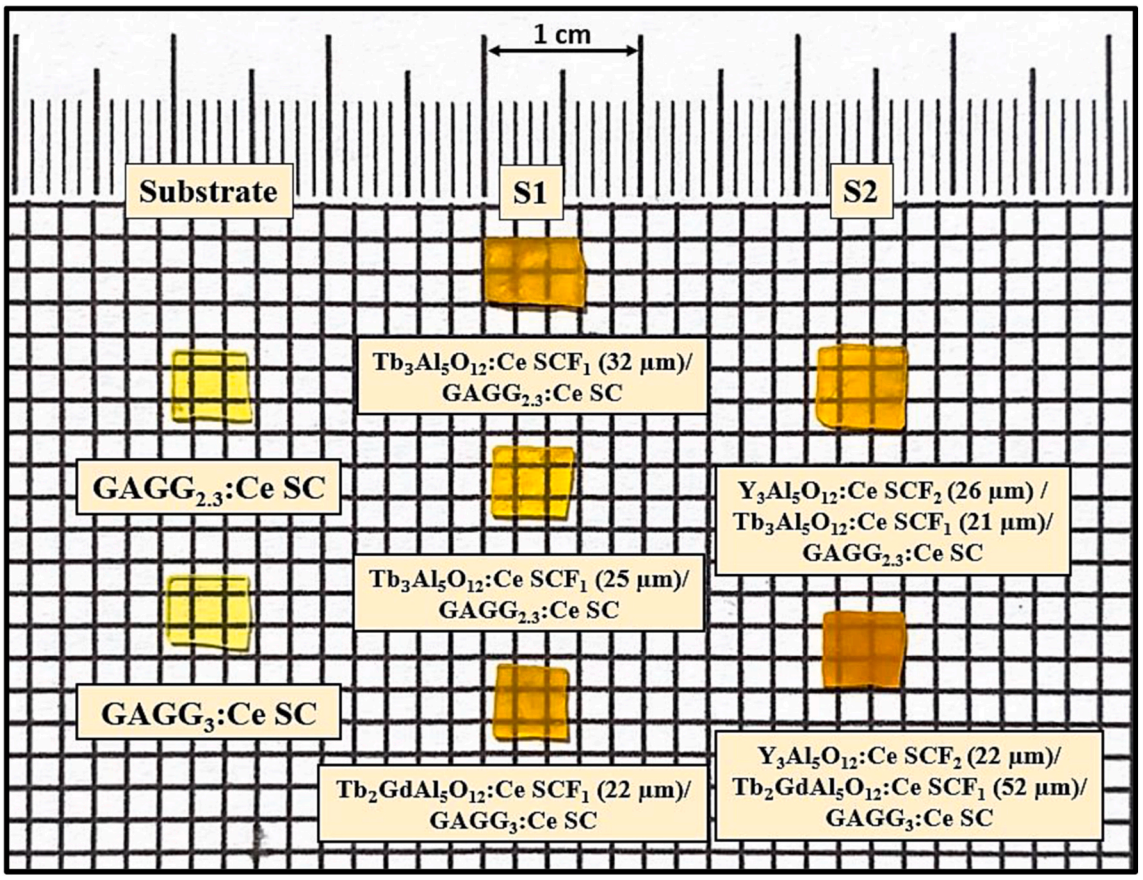

Fig. 1. Photo of $GAGG_{2.3}$:Ce and $GAGG_{3.0}$:Ce SCs substrates and grown on their base S1 and S2 composite scintillators with different film's thicknesses.

Table 1
The content, thickness, LY and decay times $t_{1/e}$, $t_{1/10}$ and $t_{1/20}$ of the SCFs and crystals parts of composite scintillators under α-particles excitation by ^{239}Pu (5.15 MeV) source in comparison with reference YAG:Ce SCF sample with a LY of 2650 photons/MeV.

N	Samples	SCF/substrate thickness, μm	$t_{1/e}$, ns	$t_{1/10}$, ns	$t_{1/20}$, ns	LY, %
1	YAG:Ce SCF	55	–	–	–	100
2	$GAGG_{2.3}$:Ce	500	326	775	1097	362
3	$GAGG_{3.0}$:Ce	500	243	619	918	314
4	TbAG:Ce SCF_1/$GAGG_{2.3}$:Ce SC	32/500	420	2387	3532	163
5	TbAG:Ce SCF_1/$GAGG_{2.3}$:Ce SC	25/500	348	1621	2400	145
6	Tb_2GdAG:Ce SCF_1/$GAGG_{3.0}$:Ce SC	22/500	229	593	880	79
7	YAG:Ce SCF_2/TbAG:Ce SCF_1/$GAGG_{2.3}$:Ce SC	26/21/500	54	140	203	54
8	YAG:Ce SCF_2/Tb_2GdAG:Ce SCF_1/$GAGG_{3.0}$:Ce SC	15/52/500	106	370	721	15

3. Results and discussion

Absorption spectra. The absorption spectra of S1 and S2 sets of composite scintillators, were compared with the spectra of $GAGG_{2.3}$:Ce and $GAGG_{3.0}$:Ce substrates on Fig. 2. Tb^{3+} and Gd^{3+} ions in the different parts of SCF and crystal scintillators possesses several lines in absorption spectra corresponded to these cations. Specifically, the bands in the substrate and SCF spectra peaked at 275 and 313–315 nm can be attributed to the $^8S_{7/2} \rightarrow {}^6I_{3/2\text{-}7/2}$ transitions of Gd^{3+} ions (Fig. 2, curves 6, 7) [21]. The bands centered around ~270 nm belong to the low spin-allowed (LS) 4f→5d_2 and 4f→5d_1 absorption transitions of Tb^{3+} ions. Also, low intensity peaks positioned at 372–378 nm can be attributed to the $^7F_0 \rightarrow {}^5L_6$ transitions of Tb^{3+} ions [22]. The 4f-5d (^{2}E) transitions of Ce^{3+} ions are responsible for the absorption bands within the 340 nm and 438–444 nm range (designated as E_2 and E_1 bands, respectively) for all SCFs scintillators, as well as $GAGG_{2.3}$:Ce and $GAGG_{3.0}$:Ce substrates. Other Ce^{3+} absorption bands in these scintillators are situated below 230 nm and are associated with the 4f-5d (T_{2g}) transitions [23,24].

The absorption spectra of composite scintillators produced from a PbO-based flux show an extra wide band peaking at around 255 nm (Fig. 2). The intensity of this band is highly dependent on the SCF thickness and cannot be observed in the absorption spectra of $GAGG_x$:Ce SC substrates. The $O^{2-} \rightarrow Ce^{4+}$ charge transfer transitions (CTTs) in the S1 and S2 sets of composite scintillators are connected to the presence of this band. This result is coherent with the creation of these bands in YAG:Ce, TbAG:Ce, LuAG:Ce, and $GAGG_x$:Ce crystals and films doped with two-charged A^{2+} ions (A = Mg, Ca, Ba, and Sr) [25–27]. Therefore,

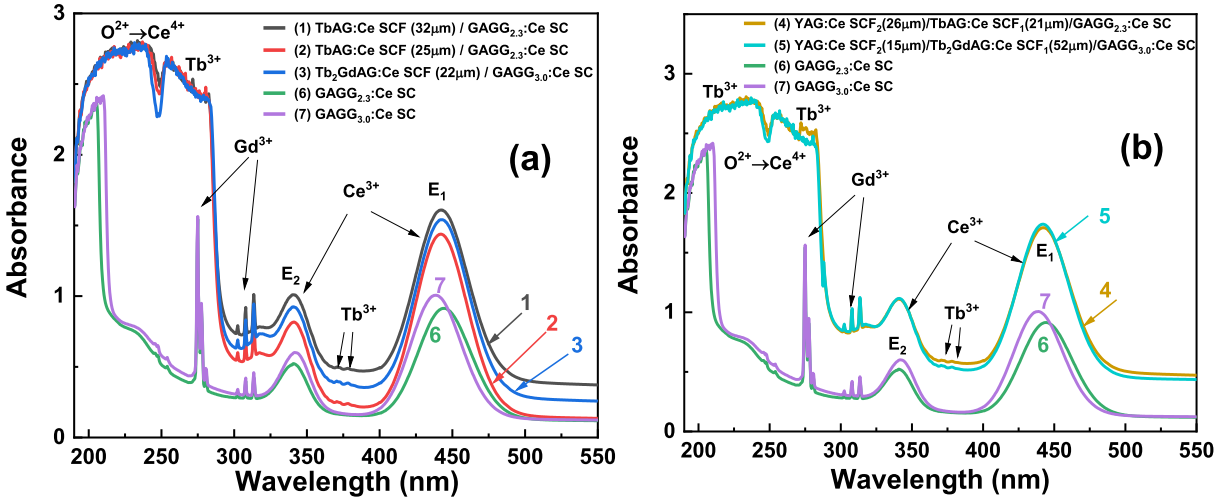

Fig. 2. Absorption spectra of both sets S1 and S2 composite scintillators in comparison with absorption spectra of $GAGG_{2.3}$:Ce and $GAGG_{3.0}$:Ce substrates.

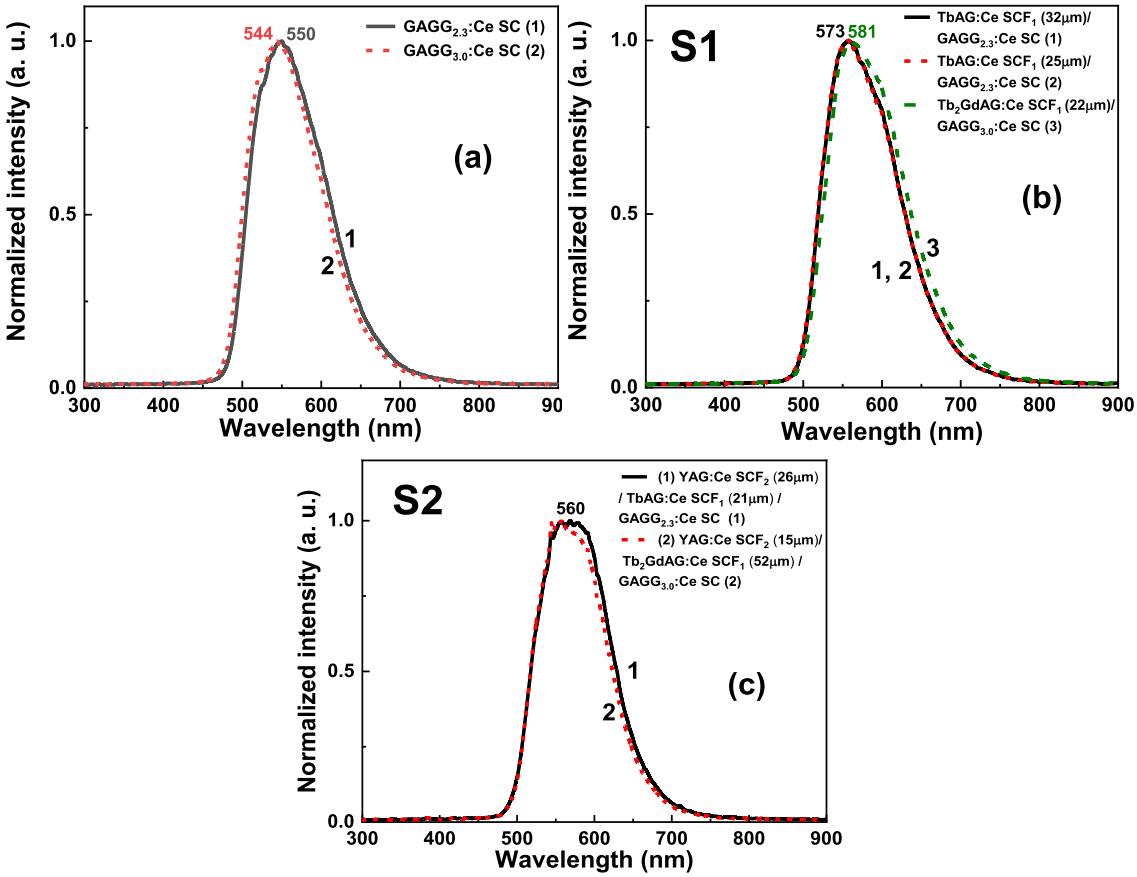

Fig. 3. RT normalized CL spectra of substrates $GAGG_{2.3}$:Ce and $GAGG_{3.0}$:Ce SCs (a), and both sets of S1 (b) and S2 (c) of composite scintillators.

the Pb^{2+} dopant is responsible for the creation of the Ce^{4+} state in the studied SCFs, grown from PbO based flux. In SCFs of different oxides produced using PbO flux, the formation of the Ce^{4+} state is energetically beneficial for the local charge and volume adjustment of the Pb^{2+} excess [28]. Notably, the wide $O^{2+}\rightarrow Ce^{4+}$ absorption bands at 255 nm closely match with the absorption band of Gd^{3+} ions [25–27].

Cathodoluminescence (CL) spectra. The normalized RT CL spectra of $GAGG_{2.3}$:Ce and $GAGG_{3.0}$:Ce SC substrates in comparison with two sets of composite scintillators S1 and S2 with different film thickness and compound of top SCF are shown in Fig. 3. The CL spectra provide useful information about the luminescence characteristics of Ce^{3+} ions in different garnet hosts according to their composition. Emission bands peaking at 550 and 544 nm (Fig. 3a) are visible in the CL spectra of the substrates $GAGG_{2.3}$:Ce and $GAGG_{3.0}$:Ce, respectively. As was previously mentioned, these bands correlate with the 5 $d^1\rightarrow 4f$ ($^2F_{5/2;7/2}$) transitions of Ce^{3+} ions in the respective garnet hosts. When the Ga content in the respective SCs increases, the peak positions of the Ce^{3+} luminescence bands in $GAGG_x$:Ce crystals are blue-shifted, and the FWHM of these bands gets slightly narrower.

The samples from S1 composite scintillator present quite different result. The large crystal field strength in the dodecahedral position of TbAG and Tb_2GdAG hosts is responsible for the more noticeable red shift of.

The CL spectra of TbAG:Ce SCF_1 and TbGdAG:Ce SCF_1 to 573–581 nm and increased FWHM of the Ce^{3+} bands in comparison with respective $GAGG_x$:Ce substrates. Slight change in the Ce^{3+} band locations in two TbAG:Ce SCF_1 samples with nominally the same content (Fig. 3b, curves 1 and 2) may be caused by variation of the Ce^{3+} concentration in these samples and the corresponding reabsorption of the luminescence of Ce^{3+} in the films with varying thicknesses [17]. This discrepancy could potentially result from slightly different conditions during the sample growths using LPE technique. Comparing it to the sample Tb_2GdAG:Ce SCF_1 grown on the substrate $GAGG_{3.0}$:Ce SC, Fig. 3b clearly demonstrates a shift towards the red region of the spectrum. Such difference is dedicated to changes in crystal field strength in Tb_2GdAG:Ce SCF_1 in comparison with TbAG:Ce garnet after additional doping with the Gd^{3+} cations [29]. Fig. 3c shows the CL spectra of the S2 set of three-layer composite scintillators centered at 560 nm, in which no significant changes were observed, considering that both samples have the same top layer composition (YAG:Ce SCF_2).

Light yield and decay times of SCFs and composite scintillators. The scintillation LY and decay kinetics of the S1 and S2 composite scintillators with varying SCF thicknesses under α-particle stimulation using ^{239}Pu (5.15 MeV) source in comparison with respective $GAGG_{2.3}$:Ce and $GAGG_{3.0}$:Ce SC substrates were presented in Figs. 4 and 5, respectively, and summarised in Table 1.

The LY of the $GAGG_{2.3}$:Ce and $GAGG_{3.0}$:Ce SC substrates under excitation by α-particles exhibits a notable sensitivity on the Ga concentration. Specifically, in comparison to the YAG:Ce SCF reference sample, the LY of mentioned substrates reduces from 362 % to 314 % when the Ga content increases from 2.3 to 3.0. However, the behavior of the scintillation decay of the $GAGG_x$:Ce SC substrates comply significantly with the change in the Ga concentration. Particularly, the GAGGx:Ce SC substrate scintillation decay kinetics are strongly accelerated as the Ga concentration increases from x = 2.3 to 3.0 (Table 1). The respective decay times $t_{1/e}$, $t_{1/10}$ and $t_{1/20}$ for $GAGG_3$:Ce SC/$GAGG_3$:Ce SC are equal to 243/326, 619/775 and 918/1097 ns, respectively. These changes of the kinetics of scintillation decay are highly useful in the design of composite scintillators, because they offer greater flexibility in choosing substrate material for simultaneous registration of scintillation decay profiles originating from the SC and SCF parts of composite scintillator.

The LY of TbAG:Ce SCFs with varying thicknesses in S1 set of composite scintillators is notable large (12.45–1.65 times) that in reference YAG:Ce SCF sample but significantly lower (up to 2.5 times) than that of its' $GAGG_{2.3}$:Ce SC substrates (Table 1). This may be explained by the creation of Ce^{4+} - Pb^{2+} pair centers in SCFs during their LPE growth and reflect the significant negative influence of Pb^{2+} contamination on LY of SCF scintillators [25–27]. It is worth noting that the LY of garnet scintillators containing Ce^{4+} -A^{2+} (Ca^{2+}, Mg^{2+}, Pb^{2+}) pairs consistently demonstrates a lower intensity compared to the LY of Ce^{3+} doped garnets [25–27] and other oxides [30,31]. However, Tb_2GdAG:Ce SCF part of S1 set of composite scintillators exhibit very lower LY in comparison with the reference YAG:Ce SCF sample and significantly (approximately by 4 times) lower LY than its respective $GAGG_{3.0}$:Ce SC substrate. This observation can be also explained by the influence of Pb^{2+} ions on the scintillation performance of Tb_2GdAG:Ce SCF.

It is important to point out that YAG:Ce SCF_2 parts of S2 set of composite scintillators have a significantly lower LY than that in S1 set of composite scintillators and substantially lower LY than that in its $GAGG_x$:Ce substrates (Table 1). This could be partly occur also due to reduced transparency of these samples (Fig. 1) and the much large segregation of Pb^{2+} opant in these epitaxial layers.

However, the mentioned low values of LY in TbAG:Ce, Tb_2GdAG:Ce and YAG:Ce SCFs scintillators is not so important for realization of main idea of this work. Even with low LY values in SCF parts of composite structures, a significant separation of the decay kinetics can be achieved in S1 and S2 sets under excitation by the different types of radiation due to the difference in the content, thickness and scintillation properties of YAG:Ce, TbAG:Ce, and TbGdAG:Ce SCFs and $GAGG_x$:Ce SC substrates (Table 1). In the following sections, we present the results of extended studies of scintillation pulse height spectra (PHS) and the decay kinetics of the studied epitaxial structures, which confirm this assumption.

Pulse height spectra (PHS). Fig. 4(a–d) show the PHS of two sets of composite scintillators based on the YAG:Ce, TbAG:Ce and Tb_2GdAG:Ce SCFs with varying SCF thicknesses (Table 1) in comparison with $GAGG_{2.3}$:Ce and $GAGG_3$:Ce SC substrates. ^{239}Pu and ^{137}Cs were employed as sources of α-particles and γ-rays, respectively, for excitation composite scintillators. Each of the main peaks in Fig. 4a and c represents the complete absorption of α-particles in comparison with an energy of 5.15 MeV.

According to the data presented in Fig. 4a-d, all $GAGG_x$:Ce (x = 2.3 and 3.0) SC substrates have a much higher scintillation efficiency than the film components of composite scintillators. This can be explained by the above-mentioned negative effects of Pb^{2+} flux-related dopants and the creation of Pb^{2+}-Ce^{4+} pairs that are responsible for the lower LY of SCF scintillators relatively to substrates with the quite close content (see Table 1).

Considering properties of both S1 and S2 sets of composite scintillators, it is worth noting that the positions of the main PHS peaks of the films and substrates clearly show that the SCF parts completely stop α-particles of ^{239}Pu source (Fig. 4a and c). However, for TbAG:Ce SCF_1 (25 μm)/$GAGG_{2.3}$:Ce SC structure, the main band after excitation by α-particles (Fig. 4a, red curve 2) is much wider and has lower pulse intensity indicating smaller LY of this sample in comparison with TbAG:Ce_1 SCF (32 μm)/$GAGG_{2.3}$:Ce SC epitaxial structure (Table 1). Likewise, the same trend is clearly visible in Fig. 4c, representing the data on S2 set of three-layered composite scintillators. Namely, the width of the peaks of YAG:Ce SCF_2/TbAG:Ce SCF_1/$GAGG_{2.3}$:Ce and YAG:Ce SCF_2/Tb_2GdAG:Ce SCF_1/$GAGG_{3.0}$:Ce structures are larger, and their position in the spectrum is in lower channels than for corresponding substrates. It should be noted also that the dependence of the band position of the main pulse has the same dependence as the pre-measured LY, shown in Table 1.

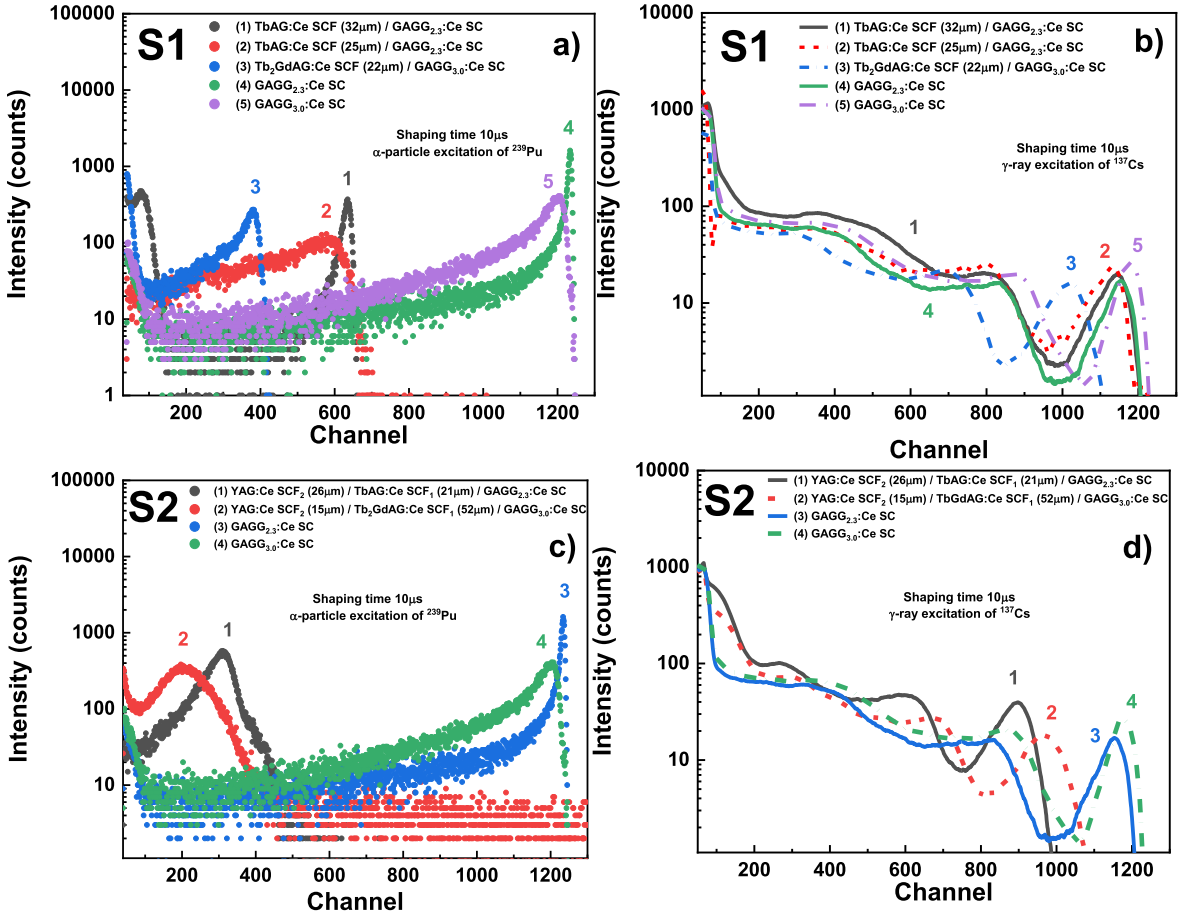

Fig. 4. PHS of the S1set of composite scintillators based on the TbAG:Ce $SCF_1/GAGG_{2.3}$:Ce SC and Tb_2GdAG:Ce $SCF_1/GAGG_{3.0}$:Ce SC epitaxial structures; and PHS of the S2 sets based on the YAG:Ce SCF_2/TbAG:Ce $SCF_1/GAGG_{2.3}$:Ce and YAG:Ce SCF_2/Tb_2GdAG:Ce $SCF_1/GAGG_{3.0}$:Ce epitaxial structures compared to $GAGG_{2.3}$:Ce and $GAGG_3$:Ce SCs substrates measured with 10 μs shaping time under α-particle excitation from ^{239}Pu (5.15 MeV) source (Fig. 4a–c) and γ-rays excitation from ^{137}Cs (662 keV) source (Fig. 4b–d).

Under γ-ray excitation from ^{137}Cs source of S1 and S2 sets of composite scintillators with different SCF thicknesses, the main PHS peaks correspond to the full absorption of γ-rays radiation with an energy of 662 keV (Fig. 4b–d). The low-energy line of a^{137}Cs source corresponds to the additional peak at 32 keV. The main peaks of all the composite scintillators and $GAGG_{2.3}$:Ce SC and $GAGG_{3.0}$:Ce SC substrates in Fig. 4b and d are located in close positions to each other. As a result, the substrate part of scintillators is mostly excited by γ-rays in S1 and S2 sets of epitaxial structures, and the influence of SCFs part on the total LY, like in case of α-particle excitation, of this composite scintillator is insignificant (Table 1).

Scintillation decay kinetics. A crucial step in the development of composite scintillators is the analysis of the differences in the scintillation decay curves of Ce^{3+} doped epitaxial structures under excitation by α- and β-particles and γ-rays. In this work, this analysis was performed on every sample from the S1 and S2 sets of composite scintillators (Fig. 5 (a–c) and 5 (e − d), respectively).

Fig. 5 shows how the precise interactions of various radiation types with the materials affect the kinetics of scintillation decay of substrates under the chosen type of excitation, which is mostly dependent on the Al/Ga ratio in the appropriate $GAGG_x$:Ce SC substrates. More specifically, use of the same excitation source, the scintillation decay kinetics of $GAGG_x$:Ce SC substrates under β-particles and γ-rays excitation become significantly accelerated with increasing Ga content (Fig. 5a–e). This optimizes the ability to separate the decay profiles from the substrate and film components of composite scintillators. However, for each type of composite scintillators, there is negligible difference in the decay patterns under simultaneous β-particles and γ-rays excitation (Fig. 5a–e).

It is worth paying attention to the slow, non-exponential decay of the SCF part of S1 composite scintillators [32,33]. Such slower and complicated decay kinetics of the Ce^{3+} luminescence is typical for Tb^{3+} based garnet hosts, where the energy transfer via the sublattice of Tb^{3+} cations is significant [32,33] in comparison with YAG:Ce reference sample, where the direct energy transfer from the host to Ce^{3+} ions dominate [34]. Note that the decay curves for alpha excitation differ from each samples of TbAG:Ce SCF_1/

$GAGG_{2.3}$:Ce SC composite. Namely, for TbAG:Ce SCF_1 sample with SCF thickness of 25 μm, a faster scintillation decay is observed in contrast to the sample with thickness of 32 μm (Fig. 5a and b). As mentioned earlier, the scintillation decay kinetics of the TbAG:Ce SCFs are strongly influenced by the admixtures of Pb^{2+} ions, entering in larger amounts to the film in the TbAG:Ce SCF1 (25 μm)/GAGG2.3:Ce SC sample, as evidenced by the respective LY value and PHS. The formation of Pb^{2+}–Ce^{4+} centers in film scintillators grown from PbO-based fluxes also contributes to a significant difference in their scintillation decay kinetics of SCF scintillators compared to substrates [30,31]. Indeed, this impurity strongly accelerates the scintillation decay of the film scintillators (Fig. 5a and b). Moreover, the Tb_2GdAG:Ce $SCF_1/GAGG_{3.0}$:Ce SC composite scintillator sample indicates even faster acceleration of the decay kinetics due to the adding Gd^{3+} cations to the matrix content (Fig. 5 c). Although doping with Gd^{3+} cations was performed primarily with the aim to reduce the SCF/substrate misfit at the LPE growth of TbAG:Ce films onto GAGG substrates, such acceleration may actually be

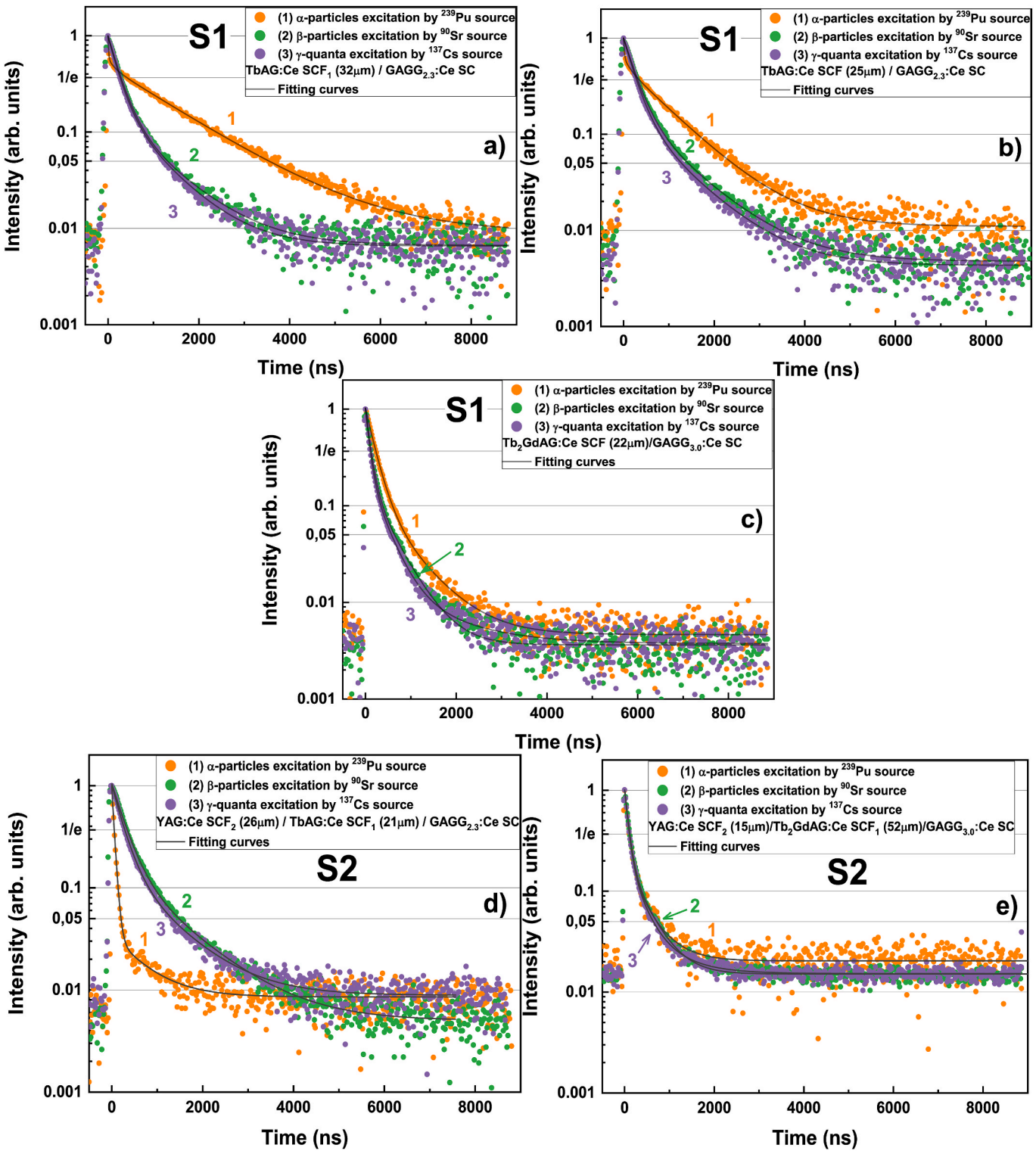

Fig. 5. Scintillation decay kinetics of S1 set of composite scintillators based on the TbAG:Ce $SCF_1/GAGG_{2.3}$:Ce SC (a, b) and Tb_2GdAG:Ce $SCF_1/GAGG_{3.0}$:Ce SC (c) epitaxial structures and S2 set of composite scintillators base on the YAG:Ce SCF_2/TbAG:Ce $SCF_1/GAGG_{2.3}$:Ce (d) and YAG:Ce SCF_2/Tb_2GdAG:Ce $SCF_1/GAGG_{3.0}$:Ce (e) epitaxial structures with different SCF thickness under excitation by α-, β-particles and γ–rays.

useful in the design of composite scintillators, as it gives an unusual scintillation decay profiles of Tb_2GdAG:Ce SCF scintillators.

Scintillation decay kinetics of tree-layered composite scintillators from the S2 series (Fig. 5d and e) are significatly different compared to the samples from the S1 series. On the one hand, the sample of YAG:Ce SCF_2/TbAG:Ce $SCF_1/GAGG_{2.3}$:Ce SC composite scintillator (Fig. 5d) has a larger difference in the decay time between the α/γ and α/β/excitations than YAG:Ce SCF_2/Tb_2GdAG:Ce $SCF_1/GAGG_{3.0}$:Ce composite (Fig. 5e). Such a big difference is caused by the previously described influence of the Al/Ga ratio on the scintillation decay kinetic of $GAGG_X$:Ce garnets, which in the case of $GAGG_{2.3}$:Ce SC is slower than that of $GAGG_{3.0}$:Ce SC substrate. Also, it is important to note the

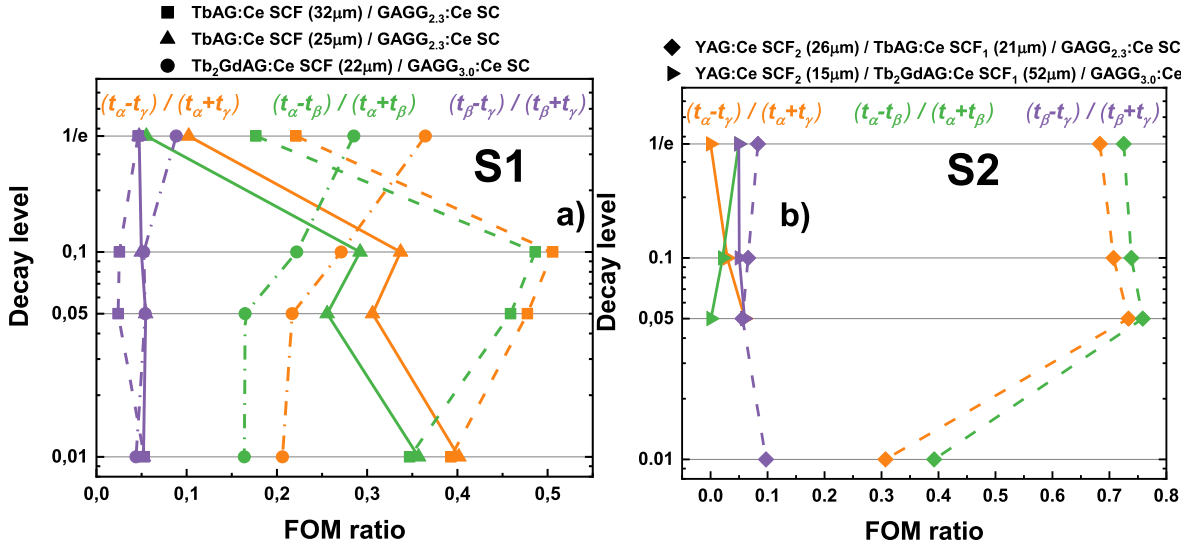

Fig. 6. FOM values for S1 and S2 sets of composite scintillators: TbAG:Ce $SCF_1/GAGG_{2.3}$:Ce SC and Tb_2GdAG:Ce $SCF_1/GAGG_{3.0}$:Ce SC (a) and YAG:Ce SCF_2/TbAG:Ce $SCF_1/GAGG_{2.3}$:Ce and YAG:Ce SCF_2/Tb_2GdAG:Ce $SCF_1/GAGG_{3.0}$:Ce SC (b) epitaxial structues under simultaneous β/γ (violet), α/β (green) and α/γ (orange) excitation. (For interpretation of the references to colour in this figure legend, the reader is referred to the Web version of this article.)

Table 2
Comparison of the decay time difference for S1 and S2 sets of composite scintillators using FOM values.

	N	Sample	$FOM_{\beta\gamma}$	$FOM_{\alpha\beta}$	$FOM_{\alpha\gamma}$
S1	**1**	$Tb_3Al_5O_{12}$:Ce SCF_1 (32 μm)/$GAGG_{2.3}$:Ce SC	0.02–0.05	0.17–0.48	0.20–0.50
	2	$Tb_3Al_5O_{12}$:Ce SCF_1 (25 μm)/$GAGG_{2.3}$:Ce SC	0.04–0.05	0.05–0.35	0.10–0.40
	3	$Tb_2GdAl_5O_{12}$:Ce $SCF_1/GAGG_{3.0}$:Ce SC	0.04–0.08	0.16–0.28	0.21–0.36
S2	**4**	$Y_3Al_5O_{12}$:Ce SCF_2/TbAG:Ce $SCF_1/GAGG_{2.3}$:Ce SC	0.05–0.10	0.40–0.76	0.30–0.73
	5	$Y_3Al_5O_{12}$:Ce $SCF_2/Tb_2GdAl_5O_{12}$:Ce $SCF_1/GAGG_{3.0}$:Ce SC	0.05–0.06	0.01–0.05	0.01–0.06

possibility of a strong impact of Pb^{2+} dopant from the PbO based flux on properties of SCF scintillators, which can significantly accelerate the kinetics of the upper part in YAG:Ce SCF_2/TbAG:Ce $SCF_1/GAGG_{2.3}$:Ce SC composite scintillator (Fig. 5d). This leads to increased differences between the scintillation decay curves for α/γ and α/β excitations compared to the sample of YAG:Ce SCF_2/Tb_2GdAG:Ce SCF_1/GAGG3.0:Ce SC composite scintillator. There is also a possibility that during the excitation of YAG:Ce SCF_2/Tb_2GdAG:Ce $SCF_1/GAGG_{3.0}$:Ce SC composite one of the deeply penetrating components of ionizing radiation excited Tb_2GdAG:Ce SCF_1, which has a faster decay time due to the presence of Gd^{3+} cations in the matrix (Fig. 5c) as compared to TbAG:Ce SCF_1 (Fig. 5a and b). All these factors result in the fact that sample YAG:Ce SCF_2/Tb_2GdAG:Ce $SCF_1/GAGG_{3.0}$:Ce SC composite scintillator has a weak ability for simultaneous separation of different types of ionizing radiation.

Under simultaneous registration of the α-, β- and γ-excitations, the difference in scintillation decay kinetic under simultaneous excitation by two radiation types was calculated using figure-of-merit (FOM) values as a quantitative measure of the separation between two scintillation signals (Eq. (1)):

$$\boldsymbol{FOM}_{\beta\gamma} = \left|\frac{(t_\beta - t_\gamma)}{(t_\beta + t_\gamma)}\right| \boldsymbol{FOM}_{\alpha\beta} = \left|\frac{(t_\alpha - t_\beta)}{(t_\alpha + t_\beta)}\right|; \boldsymbol{FOM}_{\alpha\gamma} = \left|\frac{(t_\alpha - t_\gamma)}{(t_\alpha + t_\gamma)}\right|; \quad (1)$$

As a result of calculation of FOM ratios after excitations by different types of ionizing radiation, we obtained different characteristics for both sets of samples and excitation types (Fig. 6 a, b and Table 2). Namely, Table 2 shows the calculated FOM for each of the samples during every type of ionizing radiation, considered in this work, and Fig. 6 a, b visualizes this information for both S21 and S2 sets. Comparing these values, it can be seen that $FOM_{\alpha\gamma}$ and $FOM_{\alpha\beta}$ for composite scintillators from S1 and S2 sets are large enough to provide effective separate portions of the α/γ and α/β excitations. Each of the samples indicated in this study might work as an effective composite scintillator for the registration of different types ionizing radiations taking into account the suitable measurement strategy. As an example, the sample Tb_2GdAG:Ce SCF (22 μm)/$GAGG_{3.0}$:Ce SC composite is the most effective for measuring the difference between α/β and α/γ signals at of 1/e decay level among all the solutions in this study. If considering the decay levels of 0.1 and 0.05, the sample TbAG:Ce SCF (32 μm)/$GAGG_{2.3}$:Ce SC composite scintillator is clearly the most favored for registration separation between decay kurves under α/β and α/γ excitations. Additionally, this sample has the same characteristics as the TbAG:Ce SCF (25 μm)/$GAGG_{2.3}$:Ce SC sample if take into account the registration of signals at the 1/100 of a scintillation decay level. For the samples from S2 set, the separation of different radiation types is also clearly visible for YAG:Ce SCF_2/TbAG:Ce $SCF_1/GAGG_{2.3}$:Ce structure. For this type of composite scintillator a high level of registration difference between α/γ and α/β excitations keeps almost the same throughout the whole scintillation decay levels from 1/e to 0.01. *That is the best results from all samples under study in matter of registering the difference between two types of ionizing radiations.*

Based on the results given in Fig. 6 and Table 2, we have concluded also that the difference between the scintillation decay curves of the S1 and S2 sets under the β- and γ-excitations is small for effective separation of the signals coming from these excitations. Namely, very low FOM of these samples in 0.05–0.10 range exclude septation of these two types of radiation in practical applications. It is also worth adding that due to the low LY value of the middle SCF part of YAG:Ce SCF_2/Tb_2GdAG:Ce SCF1/$GAGG_{3.0}$:Ce SC composite scintillator (Table 2), the scintillation decay curves showed a much lower intensity compared to other samples from the two sets under study. This made it difficult to record the decay kinetics at the 0.01 level, and that is why these data are not shown in Fig. 6.

4. Conclusions

The prototypes of new two-layered and three-layered composite scintillators for the simultaneous registration of different components of mixed ionization radiation fluxes have been developed on the base of epitaxial structures containing the $Y_3Al_5O_{12}$:Ce (YAG:Ce), $Tb_3Al_5O_{12}$:Ce (TbAG:Ce) and $Tb_2GdAl_5O_{12}$:Ce (Tb_2GdAG:Ce) single crystalline films (SCFs), grown by the LPE method onto the $Gd_3Al_{5-x}Ga_xO_{12}$:Ce (x = 2.3–3.0) ($GAGG_X$:Ce) single crystal (SC) substrates from the melt-solution based on the $PbO–B_2O_3$ flux. To characterize the luminescent and scintillation properties of the film and bulk crystal parts of such composite scintillators, the measurements of absorption and cathodoluminescence spectra as well as the scintillation light yield (LY) and decay kinetics under excitation by α– (^{239}Pu) and β- (^{90}Sr) particles and γ–quanta (^{137}Cs) were performed.

It was found that the formation of Pb^{2+}–Ce^{4+} pair centers in SCF scintillators results in significantly (by several times) lower LY of SCF parts of composite scintillators under α-particle excitation by ^{239}Pu source in comparison with all of the $GAGG_{2.3}$:Ce and $GAGG_{3.0}$:Ce SC substrates. However, for TbAG:Ce $SCF_1/GAGG_{2.3}$:Ce SC and Tb_2GdAG:Ce $SCF_1/GAGG_{3.0}$:Ce SC epitaxial structures, scintillation decay profiles of film scintillators under α-particles excitation significantly differ from those of the bulk crystal substrates due to: (i) the difference in the structure of emission centers in the substrates (Ce^{3+}) and films (both Ce^{3+} and Pb^{2+}–Ce^{4+}); (ii) the differences in the energy transfer processes to the Ce^{3+} ions from Tb^{3+}- and Tb^{3+}/Gd^{3+}-based garnet matrices in films and Gd^{3+} based garnet host in the substrates.

We found that the films and crystal parts of three-layered YAG:Ce SCF_2/TbAG:Ce $SCF_1/GAGG_{2.3}$:Ce and YAG:Ce SCF_2/Tb_2GdAG:Ce $SCF_1/GAGG_{3.0}$:Ce SC composite scintillators possess different scintillation decay profiles under α- and β-particles and γ-ray excitations due to the difference in the Ce^{3+} decay time in the various garnet hosts as well as due to the difference in the decay kinetics of Pb^{2+}-Ce^{4+} centers in film and Ce^{3+} centers in the substrates. We also confirmed that all the types of developed two- and three-layered composition scintillators are suitable for simultaneous registration of the different components of ionizing radiation. Namely, two-layered Tb_2GdAG:Ce SCF_1 (22 μm)/$GAGG_{3.0}$:Ce SC composite scintillators is the most effective for measuring the difference between α/β and α/γ signals at 1/e decay level while the TbAG:Ce SCF_1 (32 μm)/$GAGG_{2.3}$:Ce SC composite scintillator is better for registration the same difference at 0.1 and 0.05 decay levels. The three-layered YAG:Ce SCF_2/TbAG:Ce $SCF_1/GAGG_{2.3}$:Ce composite also showed very good ability for separation of α/β and α/γ radiation at any scintillation decay level. However, the registration differences between the β- and γ-excitations is weak in all developed types of composite scintillators. For this reason, the optimization of content of composite scintillators, the thickness of their films and crystal parts as well as application of different types of co-dopant is needed to solve the problem with simultaneous registration β/γ radiation.

The conclusions of the work shed light on the possible applications of multilayer “all-solid state” composite scintillation detectors for radiation monitoring of mixed radiation fluxes and other applications.

CRediT authorship contribution statement

Y. Syrotych: Writing – review & editing, Writing – original draft. **V. Gorbenko:** Methodology. **S. Witkiewicz-Łukaszek:** Investigation. **T. Zorenko:** Investigation. **M. Kaczmarek:** Supervision. **J. Pejchal:** Investigation, Funding acquisition. **J.A. Mares:** Investigation. **R. Kucerkova:** Investigation. **M. Nikl:** Investigation, Funding acquisition. **K. Kamada:** Methodology. **A. Yoshikawa:** Methodology. **Yu Zorenko:** Supervision, Funding acquisition, Conceptualization.

Declaration of competing interest

No known conflicts of interest.

Acknowledgements

The work was performed in the framework of Polish National Science Centre No 2022/47/I/ST8/02600 project and also supported by the Czech Science Foundation project no. 23–09743L and by the Ministry of Science and High Education of Poland in frame of Regional Excellence Initiative no RID/SP/0048/2024/01 project.

Data availability

Data will be made available on request.

References

[1] B. Ferrand, B. Chambazand, M. Couchaud, Liquid phase epitaxy: a versatile technique for the development of miniature optical components in single crystal dielectric media, Opt. Mater. 11 (1999) 101–114.
[2] E. Molva, Microchip lasers and their applications in optical microsystems, Opt. Mater. 11 (1999) 289–299.
[3] M. Klimczak, M. Malinowski, J. Sarnecki, R.J. Piramidowicz, Luminescence properties in the visible of Dy:YAG/YAG planar waveguides, Luminescence 129 (2009) 1869–1873.
[4] J.M. Robertson, M.V. Van Tol, Cathodoluminescent garnet layers, Thin Solid Films 114 (1984) 221–240.
[5] P. Schauer, O. Lalinský, M. Kucera, Overview of S(T)EM electron detectors with garnet scintillators: some potentials and limits, Microsc. Res. Tech. 84 (2021) 753–770.
[6] Z.D. Hrytskiv, Y. Zorenko, V. Gorbenko, A.D. Pedanand, V.I. Shkliarsyi, Single crystalline film screens for cathode-ray tubes: new life of television scanning optical microscopy, Radiat. Meas. 42 (2007) 933–936.
[7] A. Koch, C. Raven, P. Spanne, A. Snigirev, X-ray imaging with submicrometer resolution employing transparent luminescent screens, J. Opt. Soc. Amer. A Opt. 15 (1998) 1940–1951.
[8] T. Martin, A. Koch, Recent developments in X-ray imaging with micrometer spatial resolution, J. Synchrotron Radiat. 13 (2006) 180–194.
[9] F. Riva, P.-A. Douissard, T. Martin, F. Carla, Y.V. Zorenko, C. Dujardin, Epitaxial growth of gadolinium and lutetium-based aluminum perovskites thin film for X-rays micro-imaging applications, CrystEngComm 18 (2016) 608–615.
[10] S. Witkiewicz-Lukaszek, V. Gorbenko, T. Zorenko, O. Sidletskiy, I. Gerasymov, A. Fedorov, A. Yoshikawa, J.A. Mares, M. Nikl, Y. Zorenko, Development of composite scintillators based on single crystalline films and crystals of Ce^{3+} doped $(Lu,Gd)_3(Al,Ga)_5O_{12}$ mixed garnet compounds, Cryst. Growth Des. 18 (2018) 1834–1842.
[11] V. Gorbenko, T. Zorenko, S. Witkiewicz, K. Paprocki, O. Sidletskiy, A. Fedorov, P. Bilski, A. Twardak, Y. Zorenko, LPE growth of single crystalline film scintillators based on Ce^{3+} doped $Tb_{3-x}Gd_xAl_{5-y}Ga_yO_{12}$ mixed garnets, Crystals 7 (2017) 262.
[12] M. Nikl, Nanocomposite, Ceramic, and Thin Film Scintillators, Jenny Stanford Publishing, 2019.
[13] S. Kurosawa, A. Yoshikawa, V. Gorbenko, T. Zorenko, S. Witkiewicz-Lukaszek, A. Fedorov, Y. Zorenko, Composite scintillators based on the films and crystals of $(Lu,Gd,La)_2Si_2O_7$ pyrosilicates, IEEE Trans. Nucl. Sci. 67 (2020) 994–998.
[14] M. Globus, B. Grinyov, M. Ratner, V. Tarasov, V. Lyubinskiy, Y. Vydai, A. Ananenko, Y. Zorenko, V. Gorbenko, I. Konstankevych, New type of scintillation detectors for biological, medical, and radiation monitoring applications, IEEE Trans. Nucl. Sci. 51 (2004) 1297–1303.
[15] S. Witkiewicz-Lukaszek, V. Gorbenko, T. Zorenko, Y. Syrotych, J.A. Mares, M. Nikl, O. Sidletskiy, P. Bilski, A. Yoshikawa, Y. Zorenko, Composite detectors based on single-crystalline films and single crystals of garnet compounds, Materials 15 (2022) 1249.
[16] K. Kamada, T. Yanagida, J. Pejchal, M. Nikl, T. Endo, K. Tsutsumi, Y. Fujimoto, A. Fukabori, A. Yoshikawa, Crystal growth and scintillation properties of Ce doped $Gd_3(Ga, Al)_5O_{12}$ single crystals, IEEE Trans. Nucl. Sci. 59 (2012) 2112–2115.
[17] Y. Zorenko, P.-A. Douissard, T. Martin, F. Riva, V. Gorbenko, T. Zorenko, K. Paprocki, A. Iskalieva, S. Witkiewicz, A. Fedorov, P. Bilski, A. Twardak, Scintillating screens based on the LPE grown $Tb_3Al_5O_{12}$:Ce single crystalline films, Opt. Mater. 65 (2017) 73–81.
[18] S. Witkiewicz-Lukaszek, V. Gorbenko, T. Zorenko, Y. Syrotych, R. Kucerkova, J. A. Mares, M. Nikl, O. Sidletskiy, A. Fedorov, S. Kurosawa, K. Kamada, A. Yoshikawa, Y. Zorenko, New types of composite scintillators based on the single crystalline films and crystals of $Gd_3(Al,Ga)_5O_{12}$:Ce mixed garnets, Mater. Sci. Eng. B Solid State Mater. Adv. Technol. 264 (2021) 114909.
[19] S. Witkiewicz-Lukaszek, V. Gorbenko, T. Zorenko, K. Paprocki, O. Sidletskiy, A. Fedorov, R. Kucerkova, J.A. Mares, M. Nikl, Y. Zorenko, Epitaxial growth of composite scintillators based on $Tb_3Al_5O_{12}$: Ce single crystalline films and $Gd_3Al_{2.5}Ga_{2.5}O_{12}$: Ce crystal substrates, CrystEngComm 20 (2018) 3994–4002.
[20] P. Prusa, M. Kucera, J.A. Mares, M. Hanus, A. Beitlerova, Z. Onderisinova, M. Nikl, Scintillation properties of the Ce-doped multicomponent garnet epitaxial films, Opt. Mater. 35 (2013) 2444–2448.
[21] J.B. Gruber, M.E. Hills, C.A. Morrison, G.A. Turner, M.R. Kokta, Absorption spectra and energy levels of Gd^{3+}, Nd^{3+}, and Cr^{3+} in the garnet $Gd_3Sc_2Ga_3O_{12}$, Phys. Rev. B Condens. Matter 37 (1988) 8564–8574.

[22] D. Nakauchi, Y. Yoshida, N. Kawaguchi, T. Yanagida, Characterization of Ce-doped $RE_3Al_5O_{12}$ (RE=Tb, Dy, Ho, Er, Tm and Yb) single crystalline scintillators, J. Mater. Sci. Mater. Electron. 30 (2019) 14085–14090.
[23] P.A. Tanner, L. Fu, L. Ning, B.-M. Cheng, M.G. Brik, Soft synthesis and vacuum ultraviolet spectra of YAG:Ce^{3+} nanocrystals: reassignment of Ce^{3+} energy levels, J. Phys. Condens. Matter 19 (2007) 216213.
[24] Z. Xia, A. Meijerink, Ce^{3+}-Doped garnet phosphors: composition modification, luminescence properties and applications, Chem. Soc. Rev. 46 (2017) 275–299.
[25] S. Blahuta, A. Bessiere, B. Viana, P. Dorenbos, V. Ouspenski, Evidence and consequences of Ce^{4+} in LYSO:Ce,Ca and LYSO:Ce,Mg single crystals for medical imaging applications, IEEE Trans. Nucl. Sci. 60 (2013) 3134–3141.
[26] M. Nikl, K. Kamada, V. Babin, J. Pejchal, K. Pilarova, E. Mihokova, A. Beitlerova, K. Bartosiewicz, S. Kurosawa, A. Yoshikawa, Defect engineering in Ce-doped aluminum garnet single crystal scintillators, Cryst. Growth Des. 14 (2014) 4827–4833.
[27] I. Gerasymov, S. Witkiewicz-Lukaszek, T. Zorenko, K. Bartosiewicz, Y. Zorenko, J. Winiecki, D. Kofanov, Y. Boyaryntseva, S. Tkachenko, P. Arhipov, E. Galenin, D. Kurtsev, O. Zelenskaya, V. Alekseev, K. Lebbou, O. Sidletskiy, Effects of codoping with divalent cations on performance of YAG:Ce,C scintillator, IEEE Trans. Nucl. Sci. 70 (2023) 1362–1369.
[28] A. Dabkowski, M. Berkowski, G. Jasiołek, Czochralski crystal growth and aluminum segregation coefficient in yttrium gallium aluminum garnet, J. Cryst. Growth 71 (1985) 371–376.
[29] J. Chen, Y. Tang, X. Yi, Y. Tian, G. Ao, D. Hao, Y. Lin, S. Zhou, Fabrication of $(Tb,Gd)_3Al_5O_{12}$:Ce^{3+} phosphor ceramics for warm white light-emitting diodes application, Opt. Mater. Express 9 (2019) 3333.
[30] A. Kilian, P. Bilski, V. Gorbenko, T. Zorenko, S. Witkiewicz, K. Paprocki, Y. Zorenko, Thermoluminescent properties of cerium-doped Lu_2SO_5 and Y_2SiO_5 single crystalline films scintillators grown from PbO-B_2O_3 and Bi_2O_3 fluxes, Crystals 8 (2018) 120.
[31] Y. Zorenko, V. Gorbenko, J. Vasylkiv, T. Strzyżewski, A. Fedorov, R. Kucerkova, J. A. Mares, M. Nikl, P. Bilski, A. Twardak, Growth and luminescent properties of scintillators based on the single crystalline films of $(Lu,Gd)_3(Al,Ga)_5O_{12}$:Ce garnets, J. Lumin. 169 (2016) 828–837.
[32] M. Batentschuk, A. Osvet, G. Schierning, A. Klier, J. Schneider, A. Winnacker, Simultaneous excitation of Ce^{3+} and Eu^{3+} ions in $Tb_3Al_5O_{12}$, Radiat. Meas. 38 (2004) 539–543.
[33] X. Liu, X. Wang, Z. Wang, Selectively excited emission and Tb^{3+}→Ce^{3+} energy transfer in yttrium aluminum garnet, Phys. Rev. B Condens. Matter 39 (1989) 10633–10639.
[34] M. Moszyński, T. Ludziejewski, D. Wolski, W. Klamra, L.O. Norlin, Properties of the YAG:Ce scintillator, Nucl. Instrum. Methods Phys. Res. 345 (1994) 461–467.